Amplitude analysis of $e^+e^- \to \Upsilon(nS)\pi^+\pi^-$ at $\sqrt{s} = 10.865$ GeV

A. Garmash,[4] A. Bondar,[4] A. Kuzmin,[4] A. Abdesselam,[55] I. Adachi,[13] H. Aihara,[60] S. Al Said,[55,69] D. M. Asner,[47] V. Aulchenko,[4] T. Aushev,[21] R. Ayad,[55] A. M. Bakich,[54] A. Bala,[48] V. Bhardwaj,[38] A. Bobrov,[4] G. Bonvicini,[66] A. Bozek,[42] M. Bračko,[32,22] T. E. Browder,[12] D. Červenkov,[5] V. Chekelian,[33] A. Chen,[39] B. G. Cheon,[11] K. Chilikin,[21] R. Chistov,[21] K. Cho,[26] V. Chobanova,[33] Y. Choi,[53] D. Cinabro,[66] J. Dalseno,[33,57] Z. Doležal,[5] A. Drutskoy,[21,35] D. Dutta,[15] S. Eidelman,[4] D. Epifanov,[60] H. Farhat,[66] J. E. Fast,[47] T. Ferber,[8] A. Frey,[10] O. Frost,[8] V. Gaur,[56] S. Ganguly,[66] R. Gillard,[66] R. Glattauer,[18] Y. M. Goh,[11] B. Golob,[30,22] J. Haba,[13] T. Hara,[13] K. Hayasaka,[37] H. Hayashii,[38] X. H. He,[49] Y. Hoshi,[58] W.-S. Hou,[41] Y. B. Hsiung,[41] H. J. Hyun,[28] T. Iijima,[37,36] A. Ishikawa,[59] R. Itoh,[13] Y. Iwasaki,[13] T. Iwashita,[25] I. Jaegle,[12] T. Julius,[34] J. H. Kang,[68] E. Kato,[59] P. Katrenko,[21] H. Kawai,[6] T. Kawasaki,[44] H. Kichimi,[13] C. Kiesling,[33] D. Y. Kim,[52] J. B. Kim,[27] J. H. Kim,[26] K. T. Kim,[27] M. J. Kim,[28] Y. J. Kim,[26] K. Kinoshita,[7] J. Klucar,[22] B. R. Ko,[27] P. Kodyš,[5] S. Korpar,[32,22] P. Križan,[30,22] P. Krokovny,[4] T. Kuhr,[24] Y.-J. Kwon,[68] S.-H. Lee,[27] Y. Li,[65] L. Li Gioi,[33] J. Libby,[16] C. Liu,[50] Z. Q. Liu,[17] D. Liventsev,[13] P. Lukin,[4] D. Matvienko,[4] K. Miyabayashi,[38] H. Miyata,[44] R. Mizuk,[21,35] G. B. Mohanty,[56] A. Moll,[33,57] R. Mussa,[20] E. Nakano,[46] M. Nakao,[13] Z. Natkaniec,[42] M. Nayak,[16] E. Nedelkovska,[33] N. K. Nisar,[56] S. Nishida,[13] O. Nitoh,[63] S. Okuno,[23] S. L. Olsen,[51] W. Ostrowicz,[42] P. Pakhlov,[21,35] H. Park,[28] H. K. Park,[28] T. K. Pedlar,[31] R. Pestotnik,[22] M. Petrič,[22] L. E. Piilonen,[65] E. Ribežl,[22] M. Ritter,[33] M. Röhrken,[24] A. Rostomyan,[8] S. Ryu,[51] T. Saito,[59] Y. Sakai,[13] S. Sandilya,[56] D. Santel,[7] T. Sanuki,[59] Y. Sato,[59] O. Schneider,[29] G. Schnell,[1,14] A. J. Schwartz,[7] D. Semmler,[9] K. Senyo,[67] M. E. Sevior,[34] M. Shapkin,[19] V. Shebalin,[4] C. P. Shen,[2] T.-A. Shibata,[61] J.-G. Shiu,[41] B. Shwartz,[4] F. Simon,[33,57] Y.-S. Sohn,[68] A. Sokolov,[19] E. Solovieva,[21] S. Stanič,[45] M. Starič,[22] M. Steder,[8] T. Sumiyoshi,[62] U. Tamponi,[20,64] K. Tanida,[51] G. Tatishvili,[47] Y. Teramoto,[46] K. Trabelsi,[13] M. Uchida,[61] Y. Unno,[11] S. Uno,[13] P. Urquijo,[3] Y. Usov,[4] C. Van Hulse,[1] P. Vanhoefer,[33] G. Varner,[12] A. Vinokurova,[4] V. Vorobyev,[4] M. N. Wagner,[9] C. H. Wang,[40] P. Wang,[17] X. L. Wang,[65] M. Watanabe,[44] Y. Watanabe,[23] K. M. Williams,[65] E. Won,[27] H. Yamamoto,[59] Y. Yamashita,[43] S. Yashchenko,[8] Y. Yook,[68] C. Z. Yuan,[17] Z. P. Zhang,[50] V. Zhilich,[4] and A. Zupanc[22]

(The Belle Collaboration)

[1] *University of the Basque Country UPV/EHU, 48080 Bilbao*
[2] *Beihang University, Beijing 100191*
[3] *University of Bonn, 53115 Bonn*
[4] *Budker Institute of Nuclear Physics SB RAS and Novosibirsk State University, Novosibirsk 630090*
[5] *Faculty of Mathematics and Physics, Charles University, 121 16 Prague*
[6] *Chiba University, Chiba 263-8522*
[7] *University of Cincinnati, Cincinnati, Ohio 45221*
[8] *Deutsches Elektronen–Synchrotron, 22607 Hamburg*
[9] *Justus-Liebig-Universität Gießen, 35392 Gießen*
[10] *II. Physikalisches Institut, Georg-August-Universität Göttingen, 37073 Göttingen*
[11] *Hanyang University, Seoul 133-791*
[12] *University of Hawaii, Honolulu, Hawaii 96822*
[13] *High Energy Accelerator Research Organization (KEK), Tsukuba 305-0801*
[14] *IKERBASQUE, Basque Foundation for Science, 48011 Bilbao*
[15] *Indian Institute of Technology Guwahati, Assam 781039*
[16] *Indian Institute of Technology Madras, Chennai 600036*
[17] *Institute of High Energy Physics, Chinese Academy of Sciences, Beijing 100049*
[18] *Institute of High Energy Physics, Vienna 1050*
[19] *Institute for High Energy Physics, Protvino 142281*
[20] *INFN - Sezione di Torino, 10125 Torino*
[21] *Institute for Theoretical and Experimental Physics, Moscow 117218*
[22] *J. Stefan Institute, 1000 Ljubljana*
[23] *Kanagawa University, Yokohama 221-8686*
[24] *Institut für Experimentelle Kernphysik, Karlsruher Institut für Technologie, 76131 Karlsruhe*
[25] *Kavli Institute for the Physics and Mathematics of the Universe (WPI), University of Tokyo, Kashiwa 277-8583*
[26] *Korea Institute of Science and Technology Information, Daejeon 305-806*
[27] *Korea University, Seoul 136-713*
[28] *Kyungpook National University, Daegu 702-701*
[29] *École Polytechnique Fédérale de Lausanne (EPFL), Lausanne 1015*
[30] *Faculty of Mathematics and Physics, University of Ljubljana, 1000 Ljubljana*
[31] *Luther College, Decorah, Iowa 52101*
[32] *University of Maribor, 2000 Maribor*

[33]Max-Planck-Institut für Physik, 80805 München
[34]School of Physics, University of Melbourne, Victoria 3010
[35]Moscow Physical Engineering Institute, Moscow 115409
[36]Graduate School of Science, Nagoya University, Nagoya 464-8602
[37]Kobayashi-Maskawa Institute, Nagoya University, Nagoya 464-8602
[38]Nara Women's University, Nara 630-8506
[39]National Central University, Chung-li 32054
[40]National United University, Miao Li 36003
[41]Department of Physics, National Taiwan University, Taipei 10617
[42]H. Niewodniczanski Institute of Nuclear Physics, Krakow 31-342
[43]Nippon Dental University, Niigata 951-8580
[44]Niigata University, Niigata 950-2181
[45]University of Nova Gorica, 5000 Nova Gorica
[46]Osaka City University, Osaka 558-8585
[47]Pacific Northwest National Laboratory, Richland, Washington 99352
[48]Panjab University, Chandigarh 160014
[49]Peking University, Beijing 100871
[50]University of Science and Technology of China, Hefei 230026
[51]Seoul National University, Seoul 151-742
[52]Soongsil University, Seoul 156-743
[53]Sungkyunkwan University, Suwon 440-746
[54]School of Physics, University of Sydney, NSW 2006
[55]Department of Physics, Faculty of Science, University of Tabuk, Tabuk 71451
[56]Tata Institute of Fundamental Research, Mumbai 400005
[57]Excellence Cluster Universe, Technische Universität München, 85748 Garching
[58]Tohoku Gakuin University, Tagajo 985-8537
[59]Tohoku University, Sendai 980-8578
[60]Department of Physics, University of Tokyo, Tokyo 113-0033
[61]Tokyo Institute of Technology, Tokyo 152-8550
[62]Tokyo Metropolitan University, Tokyo 192-0397
[63]Tokyo University of Agriculture and Technology, Tokyo 184-8588
[64]University of Torino, 10124 Torino
[65]CNP, Virginia Polytechnic Institute and State University, Blacksburg, Virginia 24061
[66]Wayne State University, Detroit, Michigan 48202
[67]Yamagata University, Yamagata 990-8560
[68]Yonsei University, Seoul 120-749
[69]Department of Physics, Faculty of Science, King Abdulaziz University, Jeddah 21589

We report results on studies of the e^+e^- annihilation into three-body $\Upsilon(nS)\pi^+\pi^-$ ($n = 1, 2, 3$) final states including measurements of cross sections and the full amplitude analysis. The cross sections measured at $\sqrt{s} = 10.865$ GeV and corrected for the initial state radiation are $\sigma(e^+e^- \to \Upsilon(1S)\pi^+\pi^-) = (2.27 \pm 0.12 \pm 0.14)$ pb, $\sigma(e^+e^- \to \Upsilon(2S)\pi^+\pi^-) = (4.07 \pm 0.16 \pm 0.45)$ pb, and $\sigma(e^+e^- \to \Upsilon(3S)\pi^+\pi^-) = (1.46 \pm 0.09 \pm 0.16)$ pb. Amplitude analysis of the three-body $\Upsilon(nS)\pi^+\pi^-$ final states strongly favors $I^G(J^P)=1^+(1^+)$ quantum-number assignments for the two bottomonium-like $Z_b^\pm$ states, recently observed in the $\Upsilon(nS)\pi^\pm$ and $h_b(mP)\pi^\pm$ ($m = 1, 2$) decay channels. The results are obtained with a 121.4 fb^{-1} data sample collected with the Belle detector at the KEKB asymmetric-energy e^+e^- collider.

PACS numbers: 14.40.Pq, 13.25.Gv, 12.39.Pn

I. INTRODUCTION

Analysis of the $\Upsilon(10860)$ decays to non-$B\bar{B}$ final states has led to several surprises. Recently, the Belle Collaboration reported observation of anomalously high rates for the $e^+e^- \to \Upsilon(nS)\pi^+\pi^-$ ($n = 1, 2, 3$) [1] and $e^+e^- \to h_b(mP)\pi^+\pi^-$ ($m = 1, 2$) [2] transitions measured in the vicinity of the $\Upsilon(10860)$ peak. If the $\Upsilon(nS)$ signals are attributed entirely to the $\Upsilon(10860)$ decays, the measured partial decay widths $\Gamma[\Upsilon(10860) \to \Upsilon(nS)\pi^+\pi^-] \sim 0.5$ MeV are about two orders of magnitude larger than the typical widths for the dipion transitions amongst $\Upsilon(nS)$ states with $n \leq 4$. In addition, the rates of the $e^+e^- \to h_b(mP)\pi^+\pi^-$ processes are found to be comparable with those for $e^+e^- \to \Upsilon(nS)\pi^+\pi^-$, and hence the process with a spin flip of the heavy quark (that is, $h_b(mP)$ production) is not suppressed. These unexpected observations indicate that an exotic mechanism might contribute to the $\Upsilon(10860)$ decays. A detailed analysis of the three-body $e^+e^- \to \Upsilon(nS)\pi^+\pi^-$ and $e^+e^- \to h_b(mP)\pi^+\pi^-$ processes reported by Belle [3] revealed the presence of two charged bottomonium-like states, denoted as $Z_b(10610)^\pm$ and $Z_b(10650)^\pm$. These two resonances are observed in

the decay chains $e^+e^- \to Z_b^\pm\pi^\mp \to \Upsilon(nS)\pi^+\pi^-$ and $e^+e^- \to Z_b^\pm\pi^\mp \to h_b(mP)\pi^+\pi^-$. The non-resonant contribution is found to be sizable in the $\Upsilon(nS)\pi^+\pi^-$ channels and consistent with zero in the $h_b(mP)\pi^+\pi^-$ ones. Masses and widths of the $Z_b^\pm$ states have been measured in a two-dimensional amplitude analysis of the three-body $e^+e^- \to \Upsilon(nS)\pi^+\pi^-$ transitions [3]. Also, observation of the neutral $Z_b(10610)^0$ partner has been reported recently by Belle [4]. Although the simplified angular analysis in Ref. [5] favors the $J^P = 1^+$ assignment for the two charged Z_b states, the discrimination power against other possible combinations is not high enough to claim this assignment unequivocally.

Results of the analysis of three-body $e^+e^- \to \Upsilon(nS)\pi^+\pi^-$ processes presented in this paper are obtained utilizing Dalitz techniques that not only allow us to determine the relative fractions of intermediate components but also provide high sensitivity to the spin and parity of the Z_b states. Results on the e^+e^- annihilation to the three-body $\Upsilon(nS)\pi^+\pi^-$ final states reported here supersede those published in Ref. [1].

We use a data sample with an integrated luminosity of 121.4 fb^{-1} collected at the peak of the $\Upsilon(10860)$ resonance ($\sqrt{s} = 10.865$ GeV/c^2) with the Belle detector at the KEKB asymmetric-energy e^+e^- collider [6].

II. BELLE DETECTOR

The Belle detector [7] is a large-solid-angle magnetic spectrometer based on a 1.5 T superconducting solenoid magnet. Charged particle tracking is provided by a four-layer silicon vertex detector and a 50-layer central drift chamber (CDC) that surround the interaction point. The charged particle acceptance covers laboratory polar angles between $\theta = 17°$ and $150°$, corresponding to about 92% of the total solid angle in the center-of-mass (c.m.) frame.

Charged hadron identification is provided by dE/dx measurements in the CDC, an array of 1188 aerogel Cherenkov counters (ACC), and a barrel-like array of 128 time-of-flight scintillation counters (TOF); information from the three sub-detectors is combined to form likelihood ratios, which is then used for pion, kaon and proton discrimination. Electromagnetic showering particles are detected in an array of 8736 CsI(Tl) crystals (ECL) that covers the same solid angle as the charged particle tracking system. Electron identification in Belle is based on a combination of dE/dx measurements in the CDC, the response of the ACC, and the position, shape and total energy deposition (i.e., E/p) of the shower detected in the ECL. The electron identification efficiency is greater than 92% for tracks with $p_{\rm lab} > 1.0$ GeV/c and the hadron misidentification probability is below 0.3%. The magnetic field is returned via an iron yoke that is instrumented to detect muons and K_L^0 mesons. Muons are identified based on their penetration range and transverse scattering in the KLM detector. In the momentum region relevant to this analysis, the identification efficiency is about 90% while the probability to misidentify a pion as a muon is below 2%.

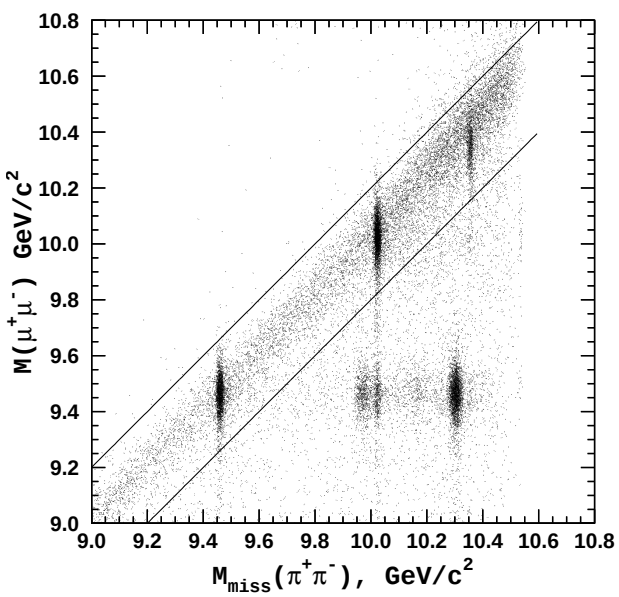

FIG. 1: Scatter plot of all the $e^+e^- \to \Upsilon(nS)\pi^+\pi^-$ candidate events passed through initial selection criteria. The region between the two diagonal lines is defined as the signal region.

We use the EvtGen event generator [8] with PHOTOS [9] for radiative corrections and a GEANT-based Monte Carlo (MC) simulation [10] to model the response of the detector and determine the acceptance. The MC simulation includes run-dependent detector performance variations and background conditions.

III. EVENT SELECTION

Charged tracks are selected with a set of track quality requirements based on the average hit residual and on the distances of closest approach to the interaction point. We require four well reconstructed tracks with a net zero charge in the event with two of them, oppositely charged, identified as muons and the other two consistent with pions. We also require that none of the four tracks be identified as an electron (electron veto).

Candidate $e^+e^- \to \Upsilon(nS)\pi^+\pi^- \to \mu^+\mu^-\pi^+\pi^-$ events are identified via the measured invariant mass of the $\mu^+\mu^-$ combination and the recoil mass, $M_{\rm miss}(\pi^+\pi^-)$, associated with the $\pi^+\pi^-$ system, defined by

$$M_{\rm miss}(\pi^+\pi^-) = \sqrt{(E_{\rm c.m.} - E^*_{\pi\pi})^2 - p^{*2}_{\pi\pi}}, \qquad (1)$$

where $E_{\rm c.m.}$ is the c.m. energy and $E^*_{\pi\pi}$ and $p^*_{\pi\pi}$ are the energy and momentum of the $\pi^+\pi^-$ system measured in the c.m. frame. The two-dimensional distribution of $M(\mu^+\mu^-)$ versus $M_{\rm miss}(\pi^+\pi^-)$ for all selected candidates is shown in Fig. 1. Events originat-

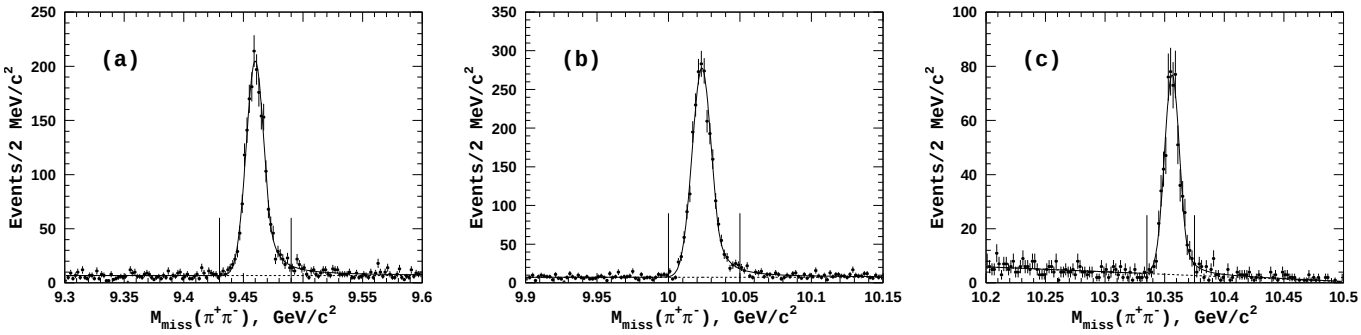

FIG. 2: Distribution of missing mass associated with the $\pi^+\pi^-$ combination for $e^+e^- \to \Upsilon(nS)\pi^+\pi^-$ candidate events in the (a) $\Upsilon(1S)$; (b) $\Upsilon(2S)$; (c) $\Upsilon(3S)$ mass region. Points with error bars are the data, the solid line is the fit, and the dashed line shows the background component. Vertical lines define the corresponding signal region.

TABLE I: Summary of results from the analysis of the $M_{\rm miss}(\pi^+\pi^-)$ distribution. Quoted uncertainty is statistical only.

Final state	$\Upsilon(1S)\pi^+\pi^-$	$\Upsilon(2S)\pi^+\pi^-$	$\Upsilon(3S)\pi^+\pi^-$
$M(\pi^+\pi^-)$ Signal, GeV/c^2	> 0.45	> 0.37	> 0.32
$N_{\rm signal}$	2090 ± 115	2476 ± 97	628 ± 41
Υ Peak, MeV/c^2	9459.9 ± 0.8	10023.4 ± 0.4	10356.2 ± 0.7
σ, MeV/c^2	8.34	7.48	6.85
$M_{\rm miss}(\pi^+\pi^-)$ Signal, GeV/c^2	$(9.430, 9.490)$	$(10.000, 10.050)$	$(10.335, 10.375)$
$N_{\rm events}$	1905	2312	635
$f_{\rm sig}$	0.937 ± 0.071	0.940 ± 0.060	0.918 ± 0.076
$M_{\rm miss}(\pi^+\pi^-)$ Sidebands, GeV/c^2	$(9.38, 9.43)$	$(9.94, 9.99)$	$(10.30, 10.33)$
	$(9.49, 9.53)$	$(10.06, 10.11)$	$(10.38, 10.41)$
$N_{\rm events}$	272	291	91

ing from the $e^+e^- \to \mu^+\mu^-\pi^+\pi^-$ process fall within a narrow diagonal band (signal region) that is defined as $|M_{\rm miss}(\pi^+\pi^-) - M(\mu^+\mu^-)| < 0.2$ GeV/c^2 (see Fig. 1). Concentrations of events within the signal region near the $\Upsilon(nS)$ nominal masses are apparent on the plot. Clusters of events below the diagonal band are mainly due to initial state radiation $e^+e^- \to \Upsilon(2S, 3S)\pi^+\pi^-\gamma$ processes and direct $e^+e^- \to \Upsilon(2S, 3S)\pi^+\pi^-$ production with a subsequent dipion transition of the $\Upsilon(2S, 3S)$ state to the ground $\Upsilon(1S)$ state. The one-dimensional $M_{\rm miss}(\pi^+\pi^-)$ projections for events in the signal region are shown in Fig. 2, where an additional requirement on the invariant mass of the $\pi^+\pi^-$ system, $M(\pi^+\pi^-)$, is imposed (see Table I) to suppress the background from photon conversion in the inner parts of the Belle detector. We perform a binned maximum likelihood fit to the $M_{\rm miss}(\pi^+\pi^-)$ distributions with a sum of a Crystal Ball function [11] for the $\Upsilon(nS)$ signal and a linear function for the combinatorial background component. The Crystal Ball function is used to account for the asymmetric shape of the $\Upsilon(nS)$ signal due to initial state radiation of soft photons. All parameters (seven in total) are free parameters of the fit. Results of the fits are shown in Fig. 2 and summarized in Table I.

For the subsequent analysis, we select events around the respective $\Upsilon(nS)$ mass peak as specified in Table I. After all the selections are applied, we are left with 1905, 2312, and 635 candidate events for the $\Upsilon(1S)\pi^+\pi^-$, $\Upsilon(2S)\pi^+\pi^-$, and $\Upsilon(3S)\pi^+\pi^-$ final state, respectively. The fractions of signal events in the selected samples are determined using results of the fit to the corresponding $M_{\rm miss}(\pi^+\pi^-)$ spectrum (see Table I). For selected events, we perform a mass-constrained fit of the $\mu^+\mu^-$ pair to the nominal mass of the corresponding $\Upsilon(nS)$ state to improve the $\Upsilon(nS)\pi$ invariant mass resolution.

IV. AMPLITUDE ANALYSIS

The e^+e^- annihilation to three-body $\Upsilon(nS)\pi^+\pi^-$ with a subsequent decay of $\Upsilon(nS) \to \mu^+\mu^-$ results in four particles that are observed in the detector; thus, there are six degrees of freedom in the system. In this analysis, we use a Lorentz-invariant form of the transition amplitude (see the Appendix) and, for visualization of fit results, we make one-dimensional projections as described below. The amplitude analysis of the $e^+e^- \to \Upsilon(nS)\pi^+\pi^-$ transitions reported here is performed by means of an unbinned maximum likelihood fit.

Before analyzing events in the signal region, one needs to determine the distribution of background events over the phase space. Samples of background events are selected in $\Upsilon(nS)$ mass sidebands and then fit to the nominal mass of the corresponding $\Upsilon(nS)$ state to match

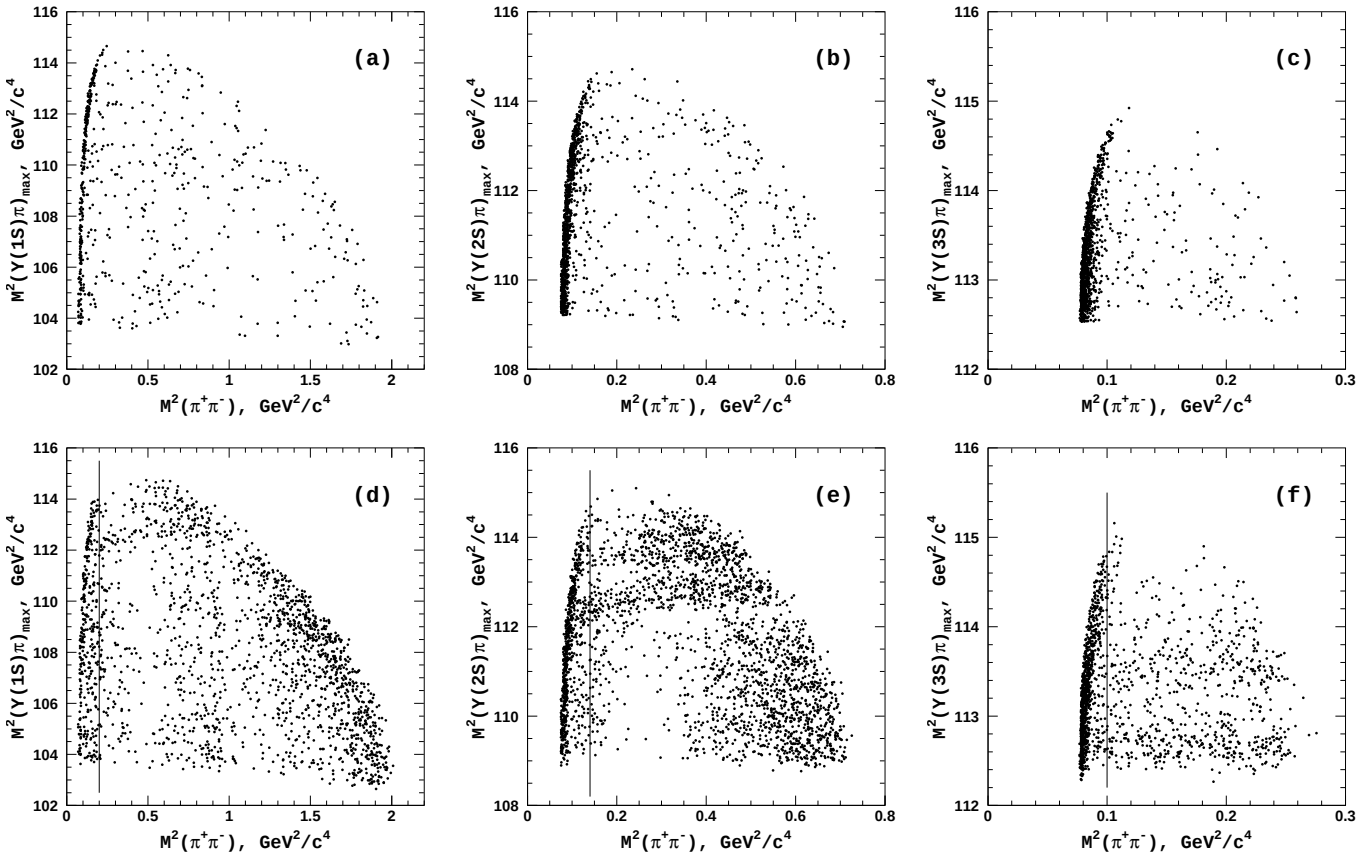

FIG. 3: Dalitz plots for $\Upsilon(nS)\pi^+\pi^-$ events in sidebands of the (a) $\Upsilon(1S)$; (b) $\Upsilon(2S)$; (c) $\Upsilon(3S)$. Dalitz plots for $\Upsilon(nS)\pi^+\pi^-$ events in the signal region of the (d) $\Upsilon(1S)$; (e) $\Upsilon(2S)$; (f) $\Upsilon(3S)$. Regions of the Dalitz plots to the left of the respective vertical line are excluded from the amplitude analyses.

the phase space boundaries for the signal. Definition of the mass sidebands and the event yields are given in Table I. Dalitz plots for the sideband events are shown in Figs. 3 (a, b, c), where $M(\Upsilon(nS)\pi)_{\rm max}$ is the maximum invariant mass of the two $\Upsilon(nS)\pi$ combinations; here the requirement on $M(\pi^+\pi^-)$ is relaxed. For visualization purposes, we plot the Dalitz distributions in terms of $M(\Upsilon(nS)\pi)_{\rm max}$ in order to combine $\Upsilon(nS)\pi^+$ and $\Upsilon(nS)\pi^-$ events. As is apparent from these distributions, there is a strong enhancement in the level of the background just above the $\pi^+\pi^-$ invariant mass threshold. This enhancement is due to conversion of photons into an e^+e^- pair in the innermost parts of the Belle detector. Due to their low momenta, conversion electrons and positrons are poorly identified by the CDC and so pass the electron veto requirement. We exclude this high background region by applying a requirement on $M(\pi^+\pi^-)$ as given in Table I. The distribution of background events in the remainder of the phase space is parametrized with the sum of a constant (that is uniform over phase space) and a term exponential in $M^2(\pi^+\pi^-)$ to account for an excess of background events in the lower $M^2(\pi^+\pi^-)$ region. In addition, in the $\Upsilon(1S)\pi^+\pi^-$ sample, we include a contribution from $\rho(770)^0 \to \pi^+\pi^-$ decays.

Figures 3(d, e, f) show Dalitz plots for events in the signal regions for the three final states being considered here. In the fit to the $e^+e^- \to \Upsilon(nS)\pi^+\pi^-$ data, we consider possible contributions from the following set of quasi-two-body modes: $Z_b(10610)^\pm\pi^\mp$, $Z_b(10650)^\pm\pi^\mp$, $\Upsilon(nS)\sigma(500)$, $\Upsilon(nS)f_0(980)$, $\Upsilon(nS)f_2(1270)$, and a nonresonant component. A detailed description of the transition amplitude is given in the Appendix.

For modes with higher $\Upsilon(nS)$ states, the available phase space is very limited, making it impossible to distinguish unambiguously between multiple scalar components in the amplitude. Thus, in the nominal model used to fit the $e^+e^- \to \Upsilon(2S)\pi^+\pi^-$ data, we fix the $f_0(980)$ amplitude at zero. In addition, in the nominal model used to fit the $e^+e^- \to \Upsilon(3S)\pi^+\pi^-$ data, we fix the $\sigma(500)$ and $f_2(1270)$ components at zero. As a result, the total numbers of fit parameters are 16, 14, and 10 for the final states with $\Upsilon(1S)$, $\Upsilon(2S)$, and $\Upsilon(3S)$, respectively. The effect of this reduction of the amplitude is considered in the evaluation of the systematic uncertainties.

In the fit to the data, we test the following assumptions on the spin and parity of the observed Z_b states:

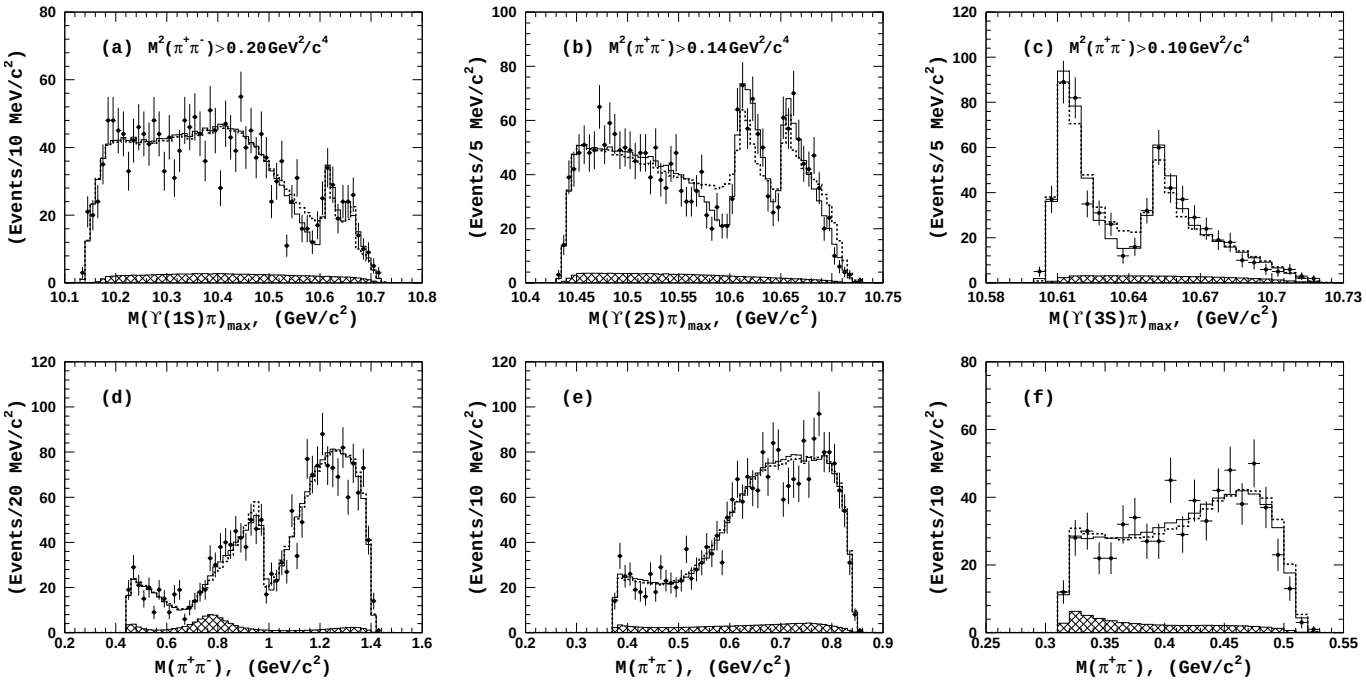

FIG. 4: Comparison of fit results with the nominal model with $J^P = 1^+$ assigned to both Z_b states (solid open histogram) and the data (points with error bars) for events in the (a, d) $\Upsilon(1S)\pi^+\pi^-$, (b, e) $\Upsilon(2S)\pi^+\pi^-$, (c, f) $\Upsilon(3S)\pi^+\pi^-$ signal region. Dashed histogram shows results of the fit with $J^P = 2^+$ assignment for the Z_b states. Hatched histograms show the estimated background components.

$J^P = 1^+$, 1^-, 2^+ and 2^-. Note that $J^P = 0^+$ and 0^- combinations are forbidden because of the observed $Z_b \to \Upsilon(nS)\pi$ and $Z_b \to h_b(mP)\pi$ decay modes, respectively. (Since the masses and the widths of two resonances measured in the $h_b(mP)\pi$ and in the $\Upsilon(nS)\pi$ [3] systems are consistent, we assume the same pair of Z_b states is observed in these decay modes.) The simplified angular analysis reported in Ref. [5] favors the $J^P = 1^+$ hypothesis; thus, our nominal model here adopts $J^P = 1^+$.

The logarithmic likelihood function $\mathcal{L}$ is

$$\mathcal{L} = -2 \sum_{\text{events}} \ln(f_{\text{sig}} S + (1 - f_{\text{sig}})B), \qquad (2)$$

where the summation is performed over all selected candidate events. The S term in Eq. 2 is formed from $|M_{\Upsilon\pi\pi}|^2$ (see the Appendix) convolved with the detector resolution, f_{sig} is the fraction of signal events in the data sample (see Table I), and B is a background density function determined from the fit to the sideband events. Both S and B are normalized to unity.

For normalization, we use a large sample of signal $e^+e^- \to \Upsilon(nS)\pi^+\pi^- \to \mu^+\mu^-\pi^+\pi^-$ MC events generated with a uniform distribution over the phase space and processed through the full detector simulation. The simulation also accounts for the beam energy spread of $\sigma = 5.3$ MeV and c.m. energy variations throughout the data taking period. The use of the full MC events for the normalization allows us to account for variations of the reconstruction efficiency over the phase space. More details can be found in Ref. [12]. Results of fits to $\Upsilon(nS)\pi^+\pi^-$ events in the signal regions with the nominal model are shown in Fig. 4, where one-dimensional projections of the data and fits are presented. In order to combine Z_b^+ and Z_b^- signals, we plot the $M(\Upsilon(nS)\pi)_{\max}$ distribution rather than individual $M(\Upsilon(nS)\pi^+)$ and $M(\Upsilon(nS)\pi^-)$ spectra. To quantify the goodness of fits, we calculate χ^2 values for one-dimensional projections shown in Fig. 4, combining any bin with fewer than nine events with its neighbor. A χ^2 variable for the multinomial distribution is then calculated as

$$\chi^2 = -2 \sum_{i=1}^{N_{\text{bins}}} n_i \ln\left(\frac{p_i}{n_i}\right), \qquad (3)$$

where n_i is the number of events observed in the i-th bin and p_i is the number of events expected from the model. For a large number of events, this formulation becomes equivalent to the standard χ^2 definition. Since we are minimizing the unbinned likelihood function, such a constructed χ^2 variable does not asymptotically follow a typical χ^2 distribution but is rather bounded by two χ^2 distributions with $(N_{\text{bins}} - 1)$ and $(N_{\text{bins}} - k - 1)$ degrees of freedom [13], where k is the number of fit parameters. Because it is bounded by two χ^2 distributions, it remains a useful statistic to estimate the goodness of the fits. Results are presented in Table II. For all final states, the nominal model provides a good description of the data.

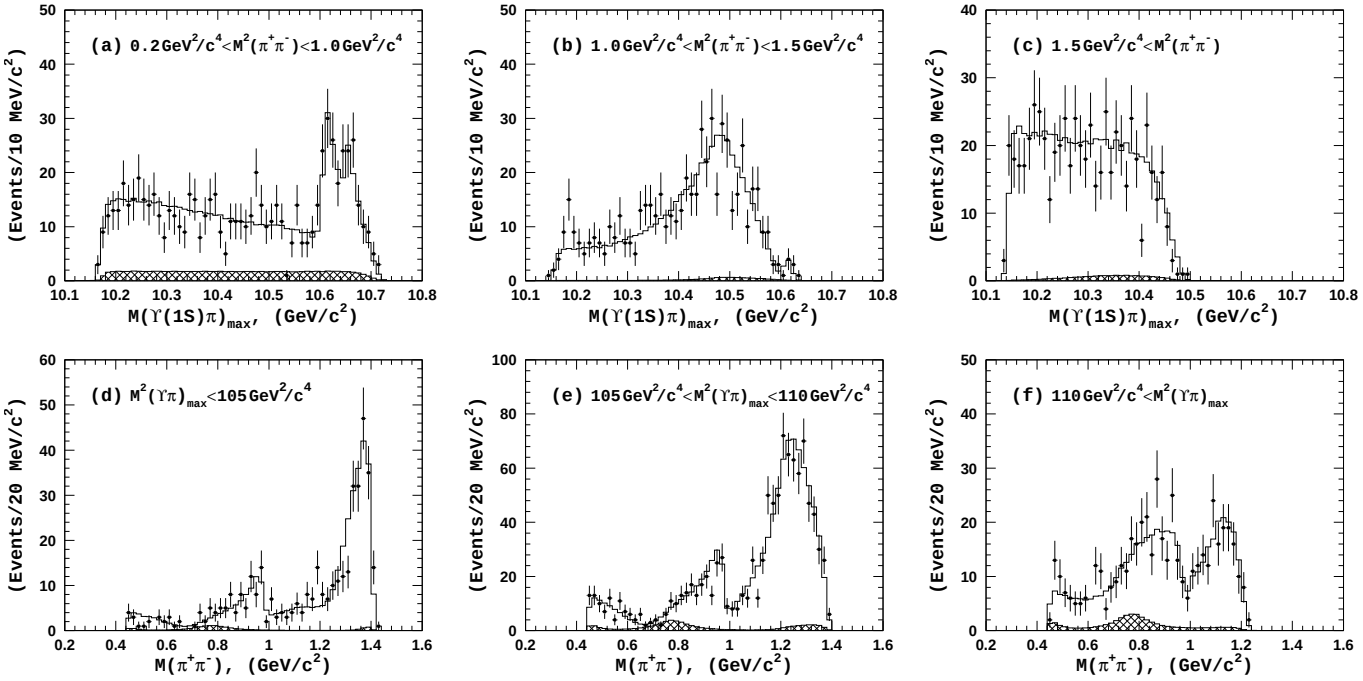

FIG. 5: A detailed comparison of fit results with the nominal model (open histogram) with the data (points with error bars) for events in the $\Upsilon(1S)\pi^+\pi^-$ signal region. Hatched histograms show the estimated background components.

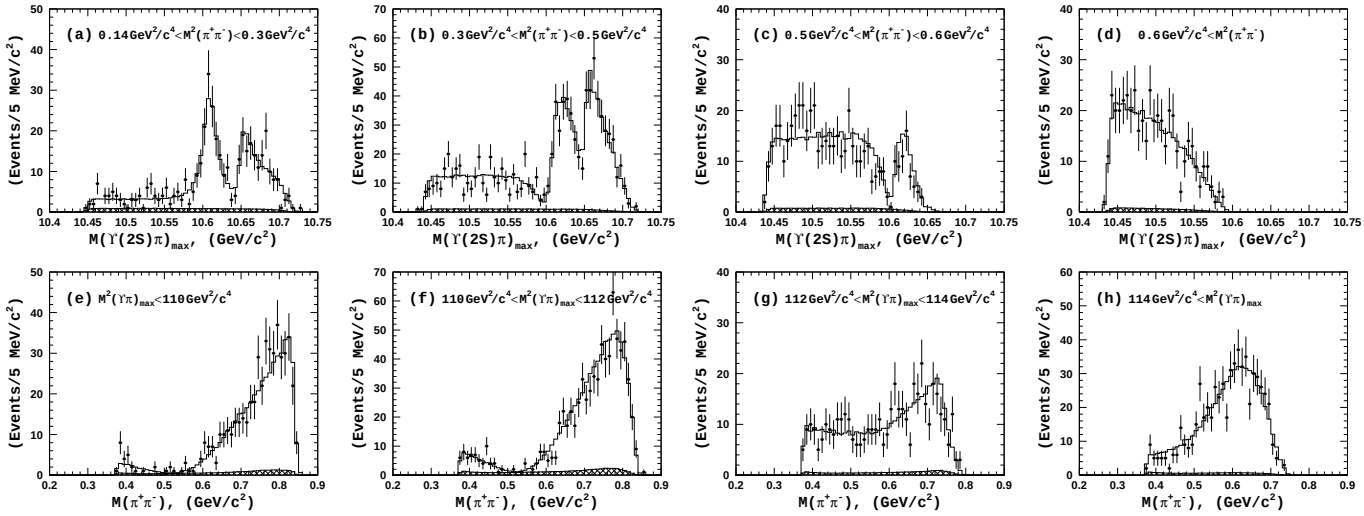

FIG. 6: A detailed comparison of fit results with the nominal model (open histogram) with the data (points with error bars) for events in the $\Upsilon(2S)\pi^+\pi^-$ signal region. Hatched histograms show the estimated background components.

A more detailed comparison of the fit results and the data is shown in Figs. 5-7, where mass projections for various regions of the Dalitz plots are presented. In addition, comparison of the angular distributions for the $Z_b(10610)$ region ($10605\ \mathrm{MeV}/c^2 < M(\Upsilon(nS)\pi)_{\max} < 10635\ \mathrm{MeV}/c^2$), the $Z_b(10650)$ region ($10645\ \mathrm{MeV}/c^2 < M(\Upsilon(nS)\pi)_{\max} < 10675\ \mathrm{MeV}/c^2$), and the non-resonant region ($M(\Upsilon(nS)\pi)_{\max} < 10570\ \mathrm{MeV}/c^2$) is presented for the $\Upsilon(2S)\pi^+\pi^-$ final state in Fig. 8 and for the $\Upsilon(3S)\pi^+\pi^-$ final state in Fig. 9. Here, θ_1 is the an-

TABLE II: Results of the $\chi^2/n_{\rm bins}$ calculations for one-dimensional projections shown in Fig. 4.

	$\Upsilon(1S)\pi^+\pi^-$	$\Upsilon(2S)\pi^+\pi^-$	$\Upsilon(3S)\pi^+\pi^-$
$M(\Upsilon\pi)_{\max}$	61.5/53	46.6/54	12.0/20
$M(\pi^+\pi^-)$	68.3/49	45.1/48	18.6/20

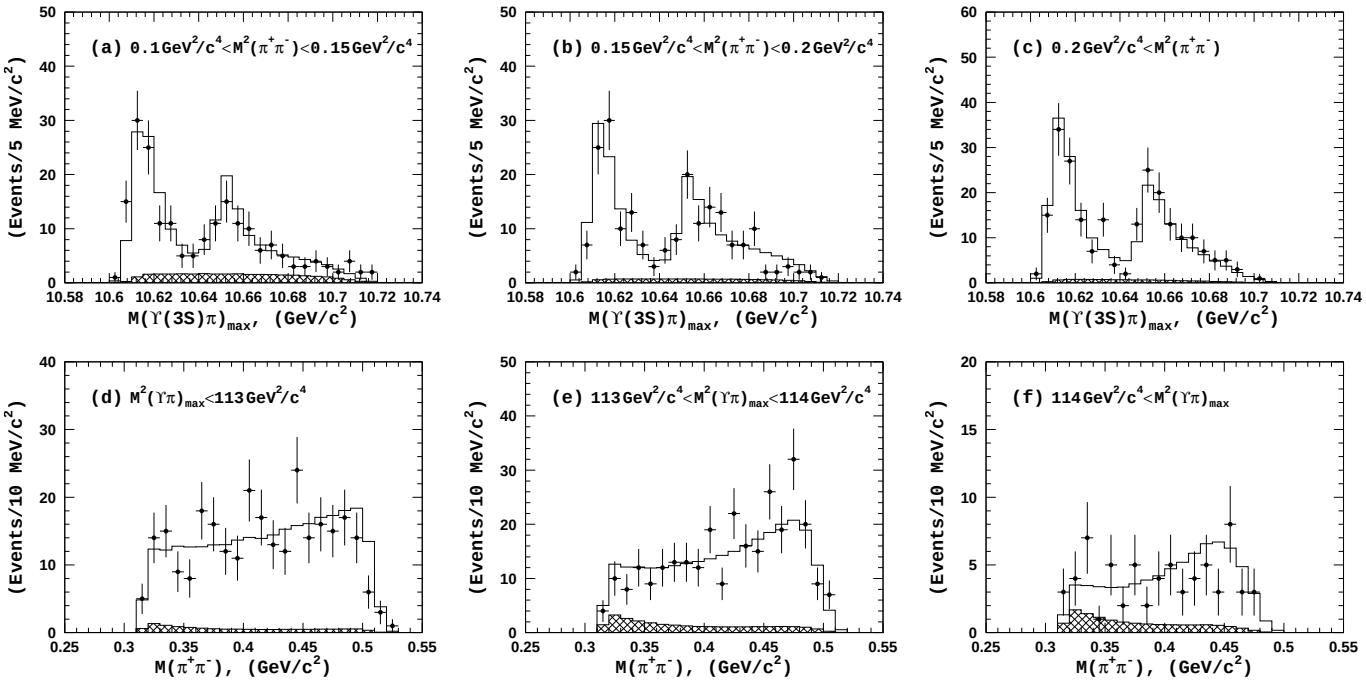

FIG. 7: A detailed comparison of fit results with the nominal model (open histogram) with the data (points with error bars) for events in the $\Upsilon(3S)\pi^+\pi^-$ signal region. Hatched histograms show the estimated background components.

gle between the prompt pion and the beam axis in the c.m. frame, $\theta^{\rm hel}_{\mu\mu}$ is the angle between the Z_b and the μ^+ momenta calculated in the $\Upsilon(nS)$ rest frame (that is, the $\Upsilon(nS) \to \mu^+\mu^-$ helicity angle), ϕ is the angle between the plane formed by the $\pi^+\pi^-$ system and the $\Upsilon(nS)$ decay plane in the Z_b rest frame, and, finally, ψ is the angle between the plane formed by the prompt pion and the beam axis and the $\Upsilon(nS)$ decay plane calculated in the Z_b rest frame.

We find that the model with $J^P = 1^+$ assigned to both Z_b states provides the best description of the data for all three three-body final states. Fits to the data with alternative J^P values assigned to the two Z_b states are compared with the nominal one in terms of the likelihood values returned by the fits. For each model, we calculate $\Delta\mathcal{L} = \mathcal{L}(J^P) - \mathcal{L}_0$ that is the difference in the likelihood values returned by the fit to a model with an alternative J^P assignment and the nominal one. Results of this study for the $\Upsilon(2S)\pi^+\pi^-$ and $\Upsilon(3S)\pi^+\pi^-$ modes (where the $Z_b\pi$ signal comprises a significant fraction of the three-body signal) are summarized in Table III. For the $\Upsilon(1S)\pi^+\pi^-$ mode, we fit the data only to models with the same J^P assigned to both Z_b states. The obtained $\Delta\mathcal{L}$ values are 64, 41, and 59 for the $J^P = 1^-$, 2^+, and 2^- models, respectively.

The best discrimination is provided by the $e^+e^- \to \Upsilon(2S)\pi^+\pi^-$ channel, where the Z_b and the underlying non-Z_b amplitudes are comparable in size, thus maximizing the relative size of the interference term. To cross-check the separation power, we perform a MC study in which we generate a large number of $\Upsilon(nS)\pi^+\pi^-$ samples, each with statistics equivalent to the data and perform fits of each pseudo-experiment with different J^P models. The obtained $\Delta\mathcal{L}$ distributions are fit to a Gaussian function (a bifurcated Gaussian function for asymmetric distributions) to estimate the probability of $\Delta\mathcal{L} > 42$. We find that alternative models with the same J^P assigned to both Z_b states are rejected at a level exceeding eight standard deviations. The comparisons of the fit result where both Z_b are assumed to be $J^P = 2^+$ states (the next best hypothesis) and the data are shown in Figs. 4, 8 and 9.

In fits with different J^P values assigned to the $Z_b(10610)$ and $Z_b(10650)$ states, the smallest $\Delta\mathcal{L}$ value is provided by the model with $Z_b(10610)$ assumed to be an 1^+ state and $Z_b(10650)$ a 2^+ state, as shown in Table III. A similar study with MC pseudo-experiments shows that

TABLE III: Results of the fit to $\Upsilon(2S)\pi^+\pi^-$ ($\Upsilon(3S)\pi^+\pi^-$) events with different J^P values assigned to the $Z_b(10610)$ and $Z_b(10650)$ states. Shown in the table is the difference in $\mathcal{L}$ values for fits to an alternative model and the nominal one.

$Z_b(10650)$ / $Z_b(10610)$	1^+	1^-	2^+	2^-
1^+	0 (0)	60 (33)	42 (33)	77 (63)
1^-	226 (47)	264 (73)	224 (68)	277 (106)
2^+	205 (33)	235 (104)	207 (87)	223 (128)
2^-	289 (99)	319 (111)	321 (110)	304 (125)

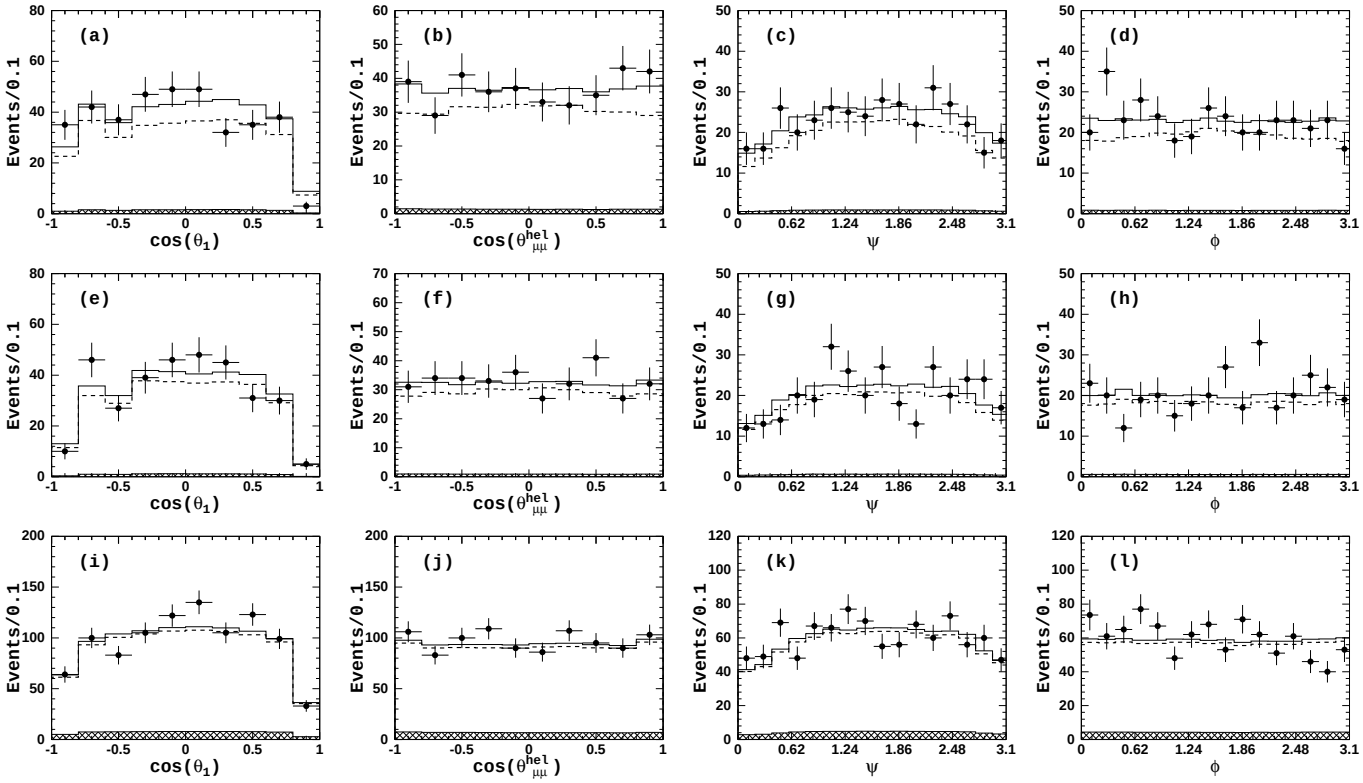

FIG. 8: Comparison of angular distributions for signal $\Upsilon(2S)\pi^+\pi^-$ events in data (points with error bars), fit with the nominal model with $J^P = 1^+$ (open histogram), and fit with $J^P = 2^+$ the model (dashed histogram). Hatched histograms show the estimated background components. The top row is for the $Z_b(10610)$ region, the middle row is for the $Z_b(10650)$ region and the bottom row is for the non-resonant region. See text for details.

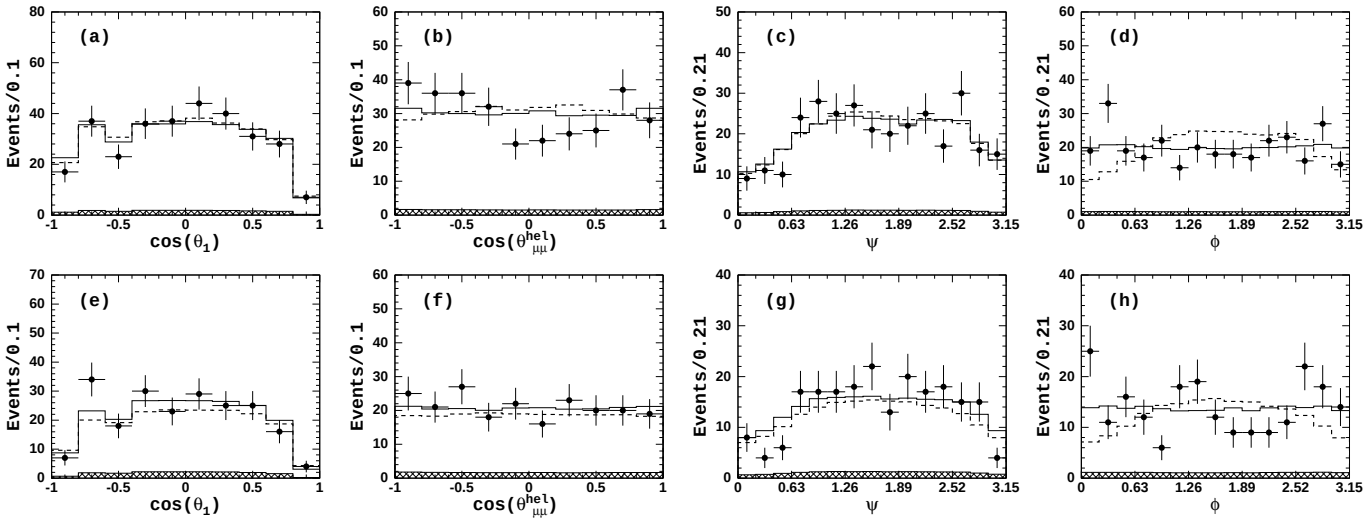

FIG. 9: Comparison of angular distributions for signal $\Upsilon(3S)\pi^+\pi^-$ events in data (points with error bars), fit with the nominal model with $J^P = 1^+$ (open histogram), and fit with the $J^P = 2^+$ model (dashed histogram). Hatched histograms show the estimated background components. The top row is for the $Z_b(10610)$ region and the bottom row is for the $Z_b(10650)$ region. See text for details.

this alternative hypothesis is rejected at a level exceeding six standard deviations.

Finally, we note that multiple solutions are found in the fit to the $\Upsilon(1S)\pi^+\pi^-$ and $\Upsilon(2S)\pi^+\pi^-$ final states. This is due to the presence of several S-wave components in the three-body amplitudes for these modes. While the

TABLE IV: Results on cross sections for three-body $e^+e^- \to \Upsilon(nS)\pi^+\pi^-$ transitions. The first quoted error is statistical and the second is systematics. The last line quotes results from our previous publication for comparison.

Final state	$\Upsilon(1S)\pi^+\pi^-$	$\Upsilon(2S)\pi^+\pi^-$	$\Upsilon(3S)\pi^+\pi^-$
Signal yield	2090 ± 115	2476 ± 97	628 ± 41
Efficiency, %	45.9	39.0	24.4
$\mathcal{B}_{\Upsilon(nS)\to\mu^+\mu^-}$, % [14]	2.48 ± 0.05	1.93 ± 0.17	2.18 ± 0.21
$\sigma^{\rm vis}_{e^+e^-\to\Upsilon(nS)\pi^+\pi^-}$, pb	$1.51 \pm 0.08 \pm 0.09$	$2.71 \pm 0.11 \pm 0.30$	$0.97 \pm 0.06 \pm 0.11$
$\sigma_{e^+e^-\to\Upsilon(nS)\pi^+\pi^-}$, pb	$2.27 \pm 0.12 \pm 0.14$	$4.07 \pm 0.16 \pm 0.45$	$1.46 \pm 0.09 \pm 0.16$
$\sigma^{\rm vis}_{e^+e^-\to\Upsilon(nS)\pi^+\pi^-}$, pb [1]	$1.61 \pm 0.10 \pm 0.12$	$2.35 \pm 0.19 \pm 0.32$	$1.44^{+0.55}_{-0.45} \pm 0.19$

overall fraction of the S-wave contribution is a well defined quantity, the individual components are strongly correlated and thus poorly separated by the fit. Because of this effect, we do not present relative phases and fractions of individual S-wave contributions except for the $\Upsilon(1S)f_0(980)$ mode, whose parameters are well defined.

V. CROSS SECTIONS

The cross sections of the three-body $e^+e^- \to \Upsilon(nS)\pi^+\pi^-$ processes are calculated using the following formula:

$$\sigma_{e^+e^-\to\Upsilon(nS)\pi^+\pi^-} = \frac{\sigma^{\rm vis}_{e^+e^-\to\Upsilon(nS)\pi^+\pi^-}}{1+\delta_{\rm ISR}} = \frac{N_{\Upsilon(nS)\pi^+\pi^-}}{L \cdot \mathcal{B}_{\Upsilon(nS)\to\mu^+\mu^-} \cdot \varepsilon_{\Upsilon(nS)\pi^+\pi^-}(1+\delta_{\rm ISR})}, \quad (4)$$

where $\sigma_{\rm vis}$ is the visible cross section. The initial state radiation (ISR) correction factor $(1+\delta_{\rm ISR}) = 0.666 \pm 0.013$ is determined using formulae given in Ref. [15], where we use the energy dependence of the $e^+e^- \to \Upsilon(nS)\pi^+\pi^-$ cross section measured in Ref. [16]. The integrated luminosity is measured to be $L = 121.4$ fb^{-1}, and the reconstruction efficiency $\varepsilon_{\Upsilon(nS)\pi^+\pi^-}$ (including trigger efficiency and final state radiation) is determined from the signal MC events generated according to the nominal model from the amplitude analysis. For the branching fractions of the $\Upsilon(nS) \to \mu^+\mu^-$ decays, the world average values are used [14]. Results of the calculations are summarized in Table IV. The Born cross section can be obtained by multiplying Eq. 4 by the vacuum polarization correction factor, $|1-\Pi|^2 = 0.9286$ [17]. The $\Upsilon(10860) \to \Upsilon(nS)\pi^+\pi^-$ branching fractions listed in Ref. [14] can be obtained by dividing our results for $\sigma^{\rm vis}$ in Table IV by the $e^+e^- \to b\bar{b}$ cross section measured at the $\Upsilon(10860)$ peak, $\sigma_{e^+e^-\to b\bar{b}}(\sqrt{s} = 10860) = 0.340 \pm 0.016$ nb [18].

The dominant sources of systematic uncertainties contributing to the measurements of cross sections for the three-body $e^+e^- \to \Upsilon(nS)\pi^+\pi^-$ transitions are given in Table V. The uncertainty in the signal yield is estimated by varying fit parameters within one standard deviations one by one and repeating the fit to the corresponding $M_{\rm miss}(\pi^+\pi^-)$ distribution. The uncertainty in the muon identification is determined using a large sample of $J/\psi \to \mu^+\mu^-$ events in data and MC and found to be 1% per muon. The uncertainty in tracking efficiency is estimated using partially reconstructed $D^{*-} \to \pi^- D^0[K^0_S\pi^+\pi^-]$ events and found to be 0.35% per a high momentum track (muons from $\Upsilon(nS) \to \mu^+\mu^-$ decays) and 1% per a lower momentum track (pions). The uncertainty in the radiative correction factor is determined from a dedicated study. It is found to be due mainly to the uncertainty in the parametrization of the energy dependence of the $e^+e^- \to \Upsilon(nS)\pi^+\pi^-$ cross section, the uncertainty in the c.m. energy and the selection criteria. All contributions are added in quadrature to obtain the overall systematic uncertainty of 6.2%, 10.9%, and 11.4% for $n = 1, 2$ and 3, respectively. Our results for $\sigma_{\rm vis}(e^+e^- \to \Upsilon(nS)\pi^+\pi^-)$ may be compared with the previous measurements by Belle performed with a data sample of 21 fb^{-1} [1] (see last line in Table IV). We find the two sets of measurements are consistent within uncertainties.

Results of the amplitude analysis are summarized in Table VI, where fractions of individual quasi-two-body modes, masses and widths of the two Z_b states, the relative phase, ϕ_Z, between the two Z_b amplitudes and fraction $c_{Z_{10610}}/c_{Z_{10650}}$ of their amplitudes are given. The fraction f_X of the total three-body signal attributed to a particular quasi-two-body intermediate state is calculated as

$$f_X = \frac{\int |\mathcal{A}_X|^2\, d\Omega}{\int |\mathcal{M}_{\Upsilon(nS)\pi\pi}|^2\, d\Omega}, \quad (5)$$

where $\mathcal{A}_X$ is the amplitude for a particular component

TABLE V: List of dominant sources of systematic uncertainties (in percent) contributing to the measurement of three-body $e^+e^- \to \Upsilon(nS)\pi^+\pi^-$ cross sections.

Final state	$\Upsilon(1S)\pi^+\pi^-$	$\Upsilon(2S)\pi^+\pi^-$	$\Upsilon(3S)\pi^+\pi^-$
$\mathcal{B}_{\Upsilon(nS)\to\mu^+\mu^-}$, [14]	2.0	8.8	9.6
Signal yield	4.5	5.3	4.9
Muon ID	2.0	2.0	2.0
Tracking	2.7	2.7	2.7
ISR correction	2.0	2.0	2.0
Luminosity	1.4	1.4	1.4
Total	6.2	10.9	11.4

TABLE VI: Summary of results of fits to $\Upsilon(nS)\pi^+\pi^-$ events in the signal regions.

Parameter	$\Upsilon(1S)\pi^+\pi^-$	$\Upsilon(2S)\pi^+\pi^-$	$\Upsilon(3S)\pi^+\pi^-$
$f_{Z_b^\mp(10610)\pi^\pm}$, %	$4.8 \pm 1.2^{+1.5}_{-0.3}$	$18.1 \pm 3.1^{+4.2}_{-0.3}$	$30.0 \pm 6.3^{+5.4}_{-7.1}$
$Z_b(10610)$ mass, MeV/c^2	$10608.5 \pm 3.4^{+3.7}_{-1.4}$	$10608.1 \pm 1.2^{+1.5}_{-0.2}$	$10607.4 \pm 1.5^{+0.8}_{-0.2}$
$Z_b(10610)$ width, MeV/c^2	$18.5 \pm 5.3^{+6.1}_{-2.3}$	$20.8 \pm 2.5^{+0.3}_{-2.1}$	$18.7 \pm 3.4^{+2.5}_{-1.3}$
$f_{Z_b^\mp(10650)\pi^\pm}$, %	$0.87 \pm 0.32^{+0.16}_{-0.12}$	$4.05 \pm 1.2^{+0.95}_{-0.15}$	$13.3 \pm 3.6^{+2.6}_{-1.4}$
$Z_b(10650)$ mass, MeV/c^2	$10656.7 \pm 5.0^{+1.1}_{-3.1}$	$10650.7 \pm 1.5^{+0.5}_{-0.2}$	$10651.2 \pm 1.0^{+0.4}_{-0.3}$
$Z_b(10650)$ width, MeV/c^2	$12.1^{+11.3+2.7}_{-4.8-0.6}$	$14.2 \pm 3.7^{+0.9}_{-0.4}$	$9.3 \pm 2.2^{+0.3}_{-0.5}$
ϕ_Z, degrees	$67 \pm 36^{+24}_{-52}$	$-10 \pm 13^{+34}_{-12}$	$-5 \pm 22^{+15}_{-33}$
$c_{Z_b(10650)}/c_{Z_b(10610)}$	$0.40 \pm 0.12^{+0.05}_{-0.11}$	$0.53 \pm 0.07^{+0.32}_{-0.11}$	$0.69 \pm 0.09^{+0.18}_{-0.07}$
$f_{\Upsilon(nS)f_2(1270)}$, %	$14.6 \pm 1.5^{+6.3}_{-0.7}$	$4.09 \pm 1.0^{+0.33}_{-1.0}$	–
$f_{\Upsilon(nS)(\pi^+\pi^-)_S}$, %	$86.5 \pm 3.2^{+3.3}_{-4.9}$	$101.0 \pm 4.2^{+6.5}_{-3.5}$	$44.0 \pm 6.2^{+1.8}_{-4.3}$
$f_{\Upsilon(nS)f_0(980)}$, %	$6.9 \pm 1.6^{+0.8}_{-2.8}$	–	–

X of the three-body amplitude $\mathcal{M}_{\Upsilon(nS)\pi\pi}$, defined in the Appendix. For amplitudes where the $\pi^+\pi^-$ system is in an S-wave, we do not calculate individual fractions for every component but present the result only for the combination $\Upsilon(nS)(\pi^+\pi^-)_S$ of all such components. The only exception is the $\Upsilon(1S)f_0(980)$ component. The statistical significance of this signal, determined as $\sqrt{\mathcal{L}_{f_0} - \mathcal{L}_0}$, where $\mathcal{L}_{f_0}$ is the likelihood value with $f_0(980)$ amplitude fixed at zero, exceeds eight standard deviations. Note, that the sum of the fit fractions for all components is not necessarily unity because of the interference. Statistical uncertainties for relative fractions of intermediate channels quoted in Table VI are determined utilizing a MC pseudo-experiment technique. For each three-body final state, we generate a large number of MC samples, each with statistics equivalent to the experimental data (including background) and with a phase space distribution according to the nominal model. Each MC sample is then fit to the nominal model and fractions f_i of contributing submodes are determined. The standard deviation of the f_i distribution is then taken as the statistical uncertainty for the fraction of the corresponding submode; see Table VI.

Combining results for the three-body cross sections from Table IV with the results of the amplitude analysis from Table VI, we calculate the product $\sigma_{Z_b^\pm\pi^\mp} \times \mathcal{B}_{\Upsilon(nS)\pi^\mp}$, where $\sigma_{Z_b^\pm\pi^\mp}$ is the cross section of the e^+e^- annihilation to $Z_b^\pm\pi^\mp$ and $\mathcal{B}_{\Upsilon(nS)\pi^\mp}$ is the branching fraction of $Z_b^\pm$ decay to $\Upsilon(nS)\pi^\pm$. For the $Z_b^\pm(10610)$, we obtain

$$\begin{aligned}
\sigma_{Z_b^\pm(10610)\pi^\mp} \times \mathcal{B}_{\Upsilon(1S)\pi^\mp} &= \quad 109 \pm 27^{+35}_{-10} \quad \text{fb} \\
\sigma_{Z_b^\pm(10610)\pi^\mp} \times \mathcal{B}_{\Upsilon(2S)\pi^\mp} &= 737 \pm 126^{+188}_{-85} \quad \text{fb} \\
\sigma_{Z_b^\pm(10610)\pi^\mp} \times \mathcal{B}_{\Upsilon(3S)\pi^\mp} &= \quad 438 \pm 92^{+92}_{-114} \quad \text{fb}, \qquad (6)
\end{aligned}$$

and for the $Z_b^\pm(10650)$, we obtain

$$\begin{aligned}
\sigma_{Z_b^\pm(10650)\pi^\mp} \times \mathcal{B}_{\Upsilon(1S)\pi^\mp} &= \quad 20 \pm 7^{+4}_{-3} \quad \text{fb} \\
\sigma_{Z_b^\pm(10650)\pi^\mp} \times \mathcal{B}_{\Upsilon(2S)\pi^\mp} &= 165 \pm 49^{+43}_{-20} \quad \text{fb} \\
\sigma_{Z_b^\pm(10650)\pi^\mp} \times \mathcal{B}_{\Upsilon(3S)\pi^\mp} &= 194 \pm 53^{+43}_{-25} \quad \text{fb}. \qquad (7)
\end{aligned}$$

The main sources of systematic uncertainties in the amplitude analysis are

- the uncertainty in parametrization of the transition amplitude. To estimate this uncertainty, we use various modifications of the nominal model and repeat the fit to the data. In particular, for the $\Upsilon(1S)\pi^+\pi^-$ and $\Upsilon(2S)\pi^+\pi^-$ channels, we modify the parametrization of the non-resonant amplitude, replacing the s_{23} dependence from linear to a $\sqrt{s_{23}}$ form and replacing the $\Upsilon(nS)f_2(1270)$ amplitude with a D-wave component in the non-resonant amplitude. For the $\Upsilon(3S)\pi^+\pi^-$ channel, we modify the nominal model by adding various components of the amplitude initially fixed at zero: a $\Upsilon(3S)f_2(1270)$ component with an amplitude and phase fixed from the fit to the $\Upsilon(1S)\pi^+\pi^-$ channel. We also fit the $\Upsilon(3S)\pi^+\pi^-$ data with the non-resonant amplitude set to be uniform. Variations in fit parameters and fractions of contributing channels determined from fits with these models are taken as an estimation of the model related uncertainty;

- multiple solutions found for the $\Upsilon(1S)\pi^+\pi^-$ and $\Upsilon(2S)\pi^+\pi^-$ modes are treated as model uncertainty, with variations in fit parameters included in the systematic uncertainty;

- uncertainty in the c.m. energy leads to uncertainty in the phase space boundaries. To estimate the associated effect on fit parameters, we generate a normalization phase space MC sample that corresponds to $E_{\rm cm} \pm 3$ MeV, where $E_{\rm cm}$ is the nominal c.m. energy, and refit;

- uncertainty in the fraction of signal events $f_{\rm sig}$ in the sample. To determine the associated uncertainties in fit parameters we vary $f_{\rm sig}$ within its error and repeat the fit to the data. We also fit the data with $f_{\rm sig}$ relaxed;

- uncertainty in the parametrization of the distribution of background events. We repeat the fit the data with a background density set to be uniform over the phase space;

- uncertainty associated with the fitting procedure. This is estimated from MC studies.

All the contributions are added in quadrature to obtain the overall systematic uncertainty. The size of the systematic uncertainty depends on the three-body $\Upsilon(nS)\pi^+\pi^-$ channel and on the particular decay submode.

VI. CONCLUSIONS

In conclusion, we have performed a full amplitude analysis of three-body $e^+e^- \to \Upsilon(nS)\pi^+\pi^-$ $(n = 1, 2, 3)$ transitions that allowed us to determine the relative fractions of various quasi-two-body components of the three-body amplitudes as well as the spin and parity of the two observed Z_b states. The favored quantum numbers are $J^P = 1^+$ for both Z_b states while the alternative $J^P = 1^-$ and $J^P = 2^\pm$ combinations are rejected at confidence levels exceeding six standard deviations. This is a substantial improvement over the previous one-dimensional angular analysis reported in Ref. [5]. This is due to the fact that the part of the amplitude most sensitive to the spin and parity of the Z_b states is the interference term between the $Z_b\pi$ and the non-resonant amplitudes. Thus, the highest sensitivity is provided by the $e^+e^- \to \Upsilon(2S)\pi^+\pi^-$ transition, where the two amplitudes $Z_b\pi$ and the non-resonant one are comparable in size. The measured values of the spin and parity of the Z_b states are in agreement with the expectations of the molecular model [19] yet do not contradict several alternative interpretations [20].

We update the measurement of the three-body $e^+e^- \to \Upsilon(nS)\pi^+\pi^-$ cross sections with significantly increased integrated luminosity compared to that in Ref. [1]. The results reported here supersede our measurements reported in Ref. [1]. We also report the first measurement of the relative fractions of the $e^+e^- \to Z_b^\mp\pi^\pm$ transitions and the first observation of the $e^+e^- \to \Upsilon(1S)f_0(980)$ transition. Finally, we find a significant contribution from the $e^+e^- \to \Upsilon(1S)(\pi^+\pi^-)_{D-\rm wave}$ amplitude but cannot attribute it unambiguously to the $\Upsilon(1S)f_2(1270)$ channel: the data can be equally well described by adding a D-wave component to the non-resonant amplitude.

Acknowledgement

We thank the KEKB group for the excellent operation of the accelerator; the KEK cryogenics group for the efficient operation of the solenoid; and the KEK computer group, the National Institute of Informatics, and the PNNL/EMSL computing group for valuable computing and SINET4 network support. We acknowledge support from the Ministry of Education, Culture, Sports, Science, and Technology (MEXT) of Japan, the Japan Society for the Promotion of Science (JSPS), and the Tau-Lepton Physics Research Center of Nagoya University; the Australian Research Council and the Australian Department of Industry, Innovation, Science and Research; Austrian Science Fund under Grant No. P 22742-N16; the National Natural Science Foundation of China under Contracts No. 10575109, No. 10775142, No. 10825524, No. 10875115, No. 10935008 and No. 11175187; the Ministry of Education, Youth and Sports of the Czech Republic under Contract No. LG14034; the Carl Zeiss Foundation, the Deutsche Forschungsgemeinschaft and the VolkswagenStiftung; the Department of Science and Technology of India; the Istituto Nazionale di Fisica Nucleare of Italy; the WCU program of the Ministry Education Science and Technology, National Research Foundation of Korea Grants No. 2011-0029457, No. 2012-0008143, No. 2012R1A1A2008330, No. 2013R1A1A3007772; the BRL program under NRF Grant No. KRF-2011-0020333, No. KRF-2011-0021196, Center for Korean J-PARC Users, No. NRF-2013K1A3A7A06056592; the BK21 Plus program and the GSDC of the Korea Institute of Science and Technology Information; the Polish Ministry of Science and Higher Education and the National Science Center; the Ministry of Education and Science of the Russian Federation, the Russian Federal Agency for Atomic Energy and the Russian Foundation for Basic Research grants RFBR 12-02-01296 and 12-02-33015; the Slovenian Research Agency; the Basque Foundation for Science (IKERBASQUE) and the UPV/EHU under program UFI 11/55; the Swiss National Science Foundation; the National Science Council and the Ministry of Education of Taiwan; and the U.S. Department of Energy and the National Science Foundation. This work is supported by a Grant-in-Aid from MEXT for Science Research in a Priority Area ("New Development of Flavor Physics") and from JSPS for Creative Scientific Research ("Evolution of Tau-lepton Physics").

Appendix: The $e^+e^- \to \Upsilon(nS)\pi^+\pi^-$ Amplitude

Here, we present a Lorentz invariant form of the amplitude for the $e^+e^- \to [\Upsilon(nS)\pi_2]\pi_1$, $\Upsilon(nS) \to \mu^+\mu^-$ transition. The amplitude might consist of several components, each describing a quasi-two-body process with a certain spin and parity of the intermediate state. The following symbols are used: K_1, K_2, P_1 and P_2 are 4-momenta for the μ^+, μ^-, π_1 and π_2, respectively;

$Q_0 = P_1 + P_2$; $Q_1 = Q_2 + P_2$; $Q_2 = K_1 + K_2$; $P_0 = Q_1 + P_1$; and ε_5 and ε_n are polarization vectors for the virtual photon and $\Upsilon(nS)$, $(n = 1, 2, 3)$, respectively. Greek indices denote 4-momenta components and run from 0 to 3. The $e^+e^- \to \Upsilon(nS)\pi^+\pi^-$ amplitude can be written as

$$\mathcal{M}_{\Upsilon(nS)\pi\pi} = \mathcal{M}_{e^+e^-\to\Upsilon(nS)\pi^+\pi^-}\mathcal{M}_{\Upsilon(nS)\to\mu^+\mu^-} = \varepsilon_5^{\mu} O_{\mu\nu}\varepsilon_n^{*\nu}\varepsilon_n^{\alpha}(\bar{u}_1\gamma_\alpha u_2) \quad (8)$$

and

$$|\mathcal{M}_{\Upsilon(nS)\pi\pi}|^2 = \varepsilon_5^{\mu'}\varepsilon_5^{\mu} O_{\mu\nu}\varepsilon_n^{*\nu}\varepsilon_n^{\alpha}\mathrm{Sp}(K_1\gamma_\alpha K_2\gamma_{\alpha'})\varepsilon_n^{*\alpha'}\varepsilon_n^{\nu'} O^*_{\mu'\nu'}, \quad (9)$$

where u_k are the muon spinors. Performing the summation over the repetitive Greek indices and neglecting the muon mass, one obtains

$$R^{\nu\nu'} = \varepsilon_n^{*\nu}\varepsilon_n^{\alpha}\mathrm{Sp}(K_1\gamma_\alpha K_2\gamma_{\alpha'})\varepsilon_n^{*\alpha'}\varepsilon_n^{\nu'} = 4(K_1^{\nu}K_2^{\nu'} + K_2^{\nu}K_1^{\nu'} - g^{\nu\nu'}(K_1\cdot K_2)), \quad (10)$$

where $(K_1 \cdot K_2) = g_{\mu\nu}K_1^{\mu}K_2^{\nu}$, and we used $\varepsilon_n^{*\nu}\varepsilon_n^{*\alpha} = g^{\nu\alpha} - \frac{Q_2^{\nu}Q_2^{\alpha}}{Q_2^2}$. Thus, we arrive at

$$|\mathcal{M}_{\Upsilon(nS)\pi\pi}|^2 = \delta_{\perp}^{\mu\mu'} O_{\mu\nu} R^{\nu\nu'} O^*_{\nu'\mu'}, \quad (11)$$

where $\delta_{\perp}^{\mu\nu} = 1$ if $\mu = \nu = 1, 2$ and $\delta_{\perp}^{\mu\nu} = 0$ otherwise. The factor $O_{\mu\nu}$ depends on the dynamics of the $e^+e^- \to \Upsilon(nS)\pi_1\pi_2$ process (see below). In what follows, we consider only the following possible contributions to the three-body amplitude: $e^+e^- \to Z_b\pi_1$, $Z_b \to \Upsilon(nS)\pi_2$ and $e^+e^- \to \Upsilon(nS)(\pi_1\pi_2)_{S,D}$, where $(\pi_1\pi_2)_{S,D}$ denotes the system of two pions in an S- and D-wave configuration, respectively. We consider the following combinations of spin and parity of the intermediate Z_b state: $J^P_{Z_b} = 1^+$, 1^-, 2^+ and 2^-. Factors $O_{\mu\nu}$ corresponding to these six amplitudes are given below.

1) $J^P_{Z_b} = 1^-$. Although both P- and F-waves are allowed for the π_2 here (and in the case of $J^P_{Z_b} = 2^-$), the F-wave is substantially suppressed by the phase space factor, so we keep only the P-wave component of the amplitude

$$O^{\mu\nu}_{\Upsilon\pi_2} = \varepsilon^*_{\alpha}\varepsilon^{\mu\alpha\gamma\rho}P_{0\gamma}Q_{1\rho}\varepsilon_{\sigma}\varepsilon^{\nu\sigma\delta\kappa}Q_{1\delta}Q_{2\kappa} = g^{\mu\nu}\Big((P_0\cdot Q_1)(Q_1\cdot Q_2) - (P_0\cdot Q_2)Q_1^2\Big) + Q_2^{\mu}P_0^{\nu}Q_1^2 - Q_2^{\mu}Q_1^{\nu}(P_0\cdot Q_1) + Q_1^{\mu}Q_1^{\nu}(P_0\cdot Q_2) - Q_1^{\mu}P_0^{\nu}(Q_1\cdot Q_2). \quad (12)$$

2) $J^P_{Z_b} = 1^+$. In this case (as well as in the case of $J^P_{Z_b} = 2^+$) S- and D-waves are allowed for the π_2. We keep only the S-wave since the D-wave is suppressed by the phase space factor. Thus

$$O^{\mu\nu}_{\Upsilon\pi_2} = (g^{\mu\alpha} + a_1P_1^{\mu}P_1^{\alpha})\varepsilon^*_{\alpha}\varepsilon_{\beta}(g^{\mu\beta} + a_2P_2^{\beta}P_2^{\nu}) = g^{\mu\nu} + a_1P_1^{\mu}P_1^{\nu} + a_2P_2^{\mu}P_2^{\nu} - \frac{Q_1^{\mu}Q_1^{\nu}}{Q_1^2}(1 - a_1(Q_1\cdot P_1) + a_2(Q_1\cdot P_2)) + a_0a_1a_2P_1^{\mu}P_2^{\nu}, \quad (13)$$

where

$$a_0 = (P_1\cdot P_2) - \frac{(Q_1\cdot P_1)(Q_1\cdot P_2)}{Q_1^2};$$
$$a_1 = \frac{(P_0\cdot Q_1) - \sqrt{P_0^2Q_1^2}}{(Q_1\cdot P_1)^2 - m_{\pi}^2Q_1^2};$$
$$a_2 = \frac{(Q_1\cdot Q_2) - \sqrt{Q_1^2Q_2^2}}{(Q_2\cdot P_2)^2 - m_{\pi}^2Q_2^2}, \quad (14)$$

and $\varepsilon^*_{\alpha}\varepsilon_{\beta} = (g_{\alpha\beta} - \frac{Q_{1\alpha}Q_{1\beta}}{Q_1^2})$.

3) $J^P_{Z_b} = 2^-$.

$$O^{\mu\nu}_{\Upsilon\pi_2} = \varepsilon^*_{\alpha\beta}\varepsilon^{\mu\alpha\gamma\rho}P_{0\gamma}Q_{1\rho}P_0^{\beta}\varepsilon_{\sigma\tau}\varepsilon^{\nu\sigma\delta\kappa}Q_{1\delta}Q_{2\kappa}Q_2^{\tau}. \quad (15)$$

Taking into account that

$$\varepsilon^*_{\alpha\beta}\varepsilon_{\sigma\delta} = \frac{1}{2}(G_{\alpha\sigma}G_{\beta\delta} + G_{\alpha\delta}G_{\beta\sigma}) - \frac{1}{3}G_{\alpha\beta}G_{\sigma\delta}, \quad (16)$$

where $G_{\alpha\beta} = g_{\alpha\beta} - \frac{Q_{1\alpha}Q_{1\beta}}{Q_1^2}$, we obtain

$$O^{\mu\nu}_{\Upsilon\pi_2} = \frac{1}{2}\Bigg[\Big(g^{\mu\nu}[(P_0\cdot Q_1)(Q_1\cdot Q_2) - (P_0\cdot Q_2)Q_1^2] + Q_2^{\mu}P_0^{\nu}Q_1^2 - Q_2^{\mu}Q_1^{\nu}(P_0\cdot Q_1) + Q_1^{\mu}Q_1^{\nu}(P_0\cdot Q_2) - Q_1^{\mu}P_0^{\nu}(Q_1\cdot Q_2)\Big)\Big((P_0\cdot Q_2) - \frac{(P_0\cdot Q_1)(Q_1\cdot Q_2)}{Q_1^2}\Big) - d^{\mu}d^{\nu}\Bigg], \quad (17)$$

where $d^{\mu} = \varepsilon^{\mu}_{\nu\alpha\beta}P_0^{\nu}Q_1^{\alpha}Q_2^{\beta}$ and $\varepsilon^{\mu}_{\nu\alpha\beta} = g^{\mu\sigma}\varepsilon_{\sigma\nu\alpha\beta}$ and $\varepsilon_{\sigma\nu\alpha\beta}$ is an antisymmetric tensor.

4) $J^P_{Z_b} = 2^+$.

$$O^{\mu\nu}_{\Upsilon\pi_2} = \varepsilon^*_{\kappa\sigma}(g^{\mu\kappa} + a_1P_1^{\mu}P_1^{\kappa})P_1^{\sigma}\varepsilon_{\alpha\beta}(g^{\alpha\nu} + a_2P_2^{\alpha}P_2^{\nu})P_2^{\beta}$$

and

$$O^{\mu\nu}_{\Upsilon\pi_2} = g^{\mu\nu}\frac{a_0}{2} + \frac{P_2^{\mu}P_1^{\nu}}{2} + P_2^{\mu}P_2^{\nu}\left(a_0a_2 - \frac{(Q_1\cdot P_1)}{2Q_1^2}\right) + P_1^{\mu}P_1^{\nu}\left(a_0a_1 - \frac{(Q_1\cdot P_2)}{2Q_1^2}\right) + \frac{1}{3}\frac{Q_1^{\mu}Q_1^{\nu}}{Q_1^4}\Bigg[(P_0\cdot Q_1)(Q_1\cdot Q_2) + 3(Q_1\cdot P_1)(Q_1\cdot P_2) - \frac{3}{2}(P_1\cdot P_2)Q_1^2 + a_2\Big((P_0\cdot Q_1)(m_{\pi}^2Q_1^2 - (Q_1\cdot P_2)^2)\Big) + a_1\Big((Q_1\cdot Q_2)(m_{\pi}^2Q_1^2 - (Q_1\cdot P_1)^2)\Big) + 3a_0Q_1^2\Big(a_1(Q_1\cdot P_1) - a_2(Q_1\cdot P_2)\Big) - a_1a_2\Big(3a_0^2Q_1^4 - (m_{\pi}^2Q_1^2 - (Q_1\cdot P_1)^2)(m_{\pi}^2Q_1^2 - (Q_1\cdot P_2)^2)\Big)\Bigg], \quad (18)$$

where factors a_0, a_1, and a_2 are the same as in Eq. 13.

In the case of production of the $\pi^+\pi^-$ system with defined spin and parity, we assume that spin structure of the $b\bar{b}$ pair is not modified and the $\pi^+\pi^-$ system is produced in an S-wave with respect to the $\Upsilon(nS)$ state and decays depending on its spin. We consider two cases: the relative angular momentum of the two pions being equal to zero (decay in an S-wave) and equal to two (decay in a D-wave). The $O^{\mu\nu}$ factor for these parts of the three-body $e^+e^- \to \Upsilon(nS)\pi^+\pi^-$ amplitude can be written as:

5) S-wave.

$$O^{\mu\nu}_S = g^{\mu\nu} + Q^\mu_0 Q^\nu_0 \frac{(P_0\cdot Q_2) - \sqrt{P_0^2 Q_2^2}}{(Q_0\cdot Q_2)^2 - Q_0^2 Q_2^2}. \qquad (19)$$

6) D-wave.

$$O^{\mu\nu}_D = O^{\mu\nu}_S \Bigg[(P_0\cdot P_1)^2 - \frac{2(P_0\cdot P_1)(Q_0\cdot P_1)(P_0\cdot Q_0)}{Q_0^2} + \frac{(P_0\cdot Q_0)^2 (Q_0\cdot P_1)^2}{Q_0^4} - \frac{1}{3}\left(P_0^2 - \frac{(P_0\cdot Q_0)}{Q_0^2}\right)\left(m_\pi^2 - \frac{(Q_0\cdot P_1)^2}{Q_0^2}\right)\Bigg]. \qquad (20)$$

The combined $O^{\mu\nu}$ in Eq. 11 is then calculated as

$$O^{\mu\nu} = a_S(s_{23}) O^{\mu\nu}_S + a_D(s_{23}) O^{\mu\nu}_D + c_{Z_1} e^{i\delta_{Z_1}} \left(a_{Z_1}(s_{12}) O^{\mu\nu}_{\Upsilon\pi_1} + a_{Z_1}(s_{13}) O^{\mu\nu}_{\Upsilon\pi_2}\right) + c_{Z_2} e^{i\delta_{Z_2}} \left(a_{Z_2}(s_{12}) O^{\mu\nu}_{\Upsilon\pi_1} + a_{Z_2}(s_{13}) O^{\mu\nu}_{\Upsilon\pi_2}\right), \qquad (21)$$

where $s_{12} = M^2(\Upsilon(nS)\pi_1)$, $s_{13} = M^2(\Upsilon(nS)\pi_2)$, and $s_{23} = M^2(\pi^+\pi^-)$ (s_{23} can be expressed via s_{12} and s_{13} but we prefer to keep it here for clarity); c_{Z_k} and δ_{z_k} are free parameters of the fit. Note that the Z_k amplitudes in Eq. 21 are symmetrized with respect to π_1 and π_2 interchange to respect isospin symmetry.

In this analysis, the S-wave part of the amplitude is comprised of the following possible modes: $\Upsilon(nS)\sigma(500)$, $\Upsilon(nS)f_0(980)$ and a non-resonant one, that is,

$$a_S(s_{23}) = c_\sigma e^{i\delta_\sigma} a_\sigma(s_{23}) + c_{f_0} e^{i\delta_{f_0}} a_{f_0}(s_{23}) + \mathcal{A}^{\rm NR}(s_{23}), \qquad (22)$$

where $a_\sigma(s_{23})$ is a Breit-Wigner function with mass and width fixed at 600 MeV/c^2 and 400 MeV, respectively; $a_{f_0}(s_{23})$ is parametrized by a Flatté function with the mass and coupling constants fixed at values defined from the analysis of $B^+ \to K^+\pi^+\pi^-$: $M(f_0(980)) =$ 950 MeV/c^2, $g_{\pi\pi} = 0.23$, $g_{KK} = 0.73$ [21]. Following the suggestion given in Refs. [22, 23], the non-resonant amplitude $\mathcal{A}^{\rm NR}(s_{23})$ is parametrized as

$$\mathcal{A}^{\rm NR}(s_{23}) = c_1^{\rm NR} e^{i\delta_1^{\rm NR}} + c_2^{\rm NR} e^{i\delta_2^{\rm NR}} s_{23}. \qquad (23)$$

The D-wave part of the three-body amplitude consists of only the $\Upsilon(nS)f_2(1270)$ mode

$$a_D(s_{23}) = c_{f_2} e^{i\delta_{f_2}} a_{f_2}(s_{23}), \qquad (24)$$

where $a_{f_2}(s_{23})$ is a Breit-Wigner function with the mass and width fixed at world average values [14]. In the study of a model related uncertainty, we also fit the data with $a_{f_2}(s_{23})$ replaced by just an s_{23} term to represent a possible D-wave component of the non-resonant amplitude. Parameters c_X, $c_k^{\rm NR}$, and phases δ_X and $\delta_k^{\rm NR}$ in Eqs. 22-24 are free parameters of the fit. Finally, terms $a_{Z_k}(s)$ in Eq. 21 are parametrized by Breit-Wigner functions with masses and widths to be determined from the fit.

Since we are sensitive to the relative phases and amplitudes only, we are free to fix one phase and one amplitude in Eq. (21). In the analysis of the $\Upsilon(1S)\pi^+\pi^-$ mode, we fix $c_1^{\rm NR} = 1$ and $\delta_1^{NR} = 0$; in the analysis of the $\Upsilon(2S)\pi^+\pi^-$ and $\Upsilon(3S)\pi^+\pi^-$ modes, we fix the amplitude and the phase of the $Z_b(10610)$ component to $c_{Z_1} = 1$ and $\delta_{Z_1} = 0$.

[1] K. F. Chen *et al.* (Belle Collaboration), Phys. Rev. Lett. **100**, 112001 (2008).
[2] I. Adachi *et al.* (Belle Collaboration), Phys. Rev. Lett. **108**, 032001 (2012).
[3] A. Bondar *et al.* (Belle Collaboration), Phys. Rev. Lett. **108**, 122001 (2012).
[4] P. Krokovny *et al.* (Belle Collaboration), Phys. Rev. D **88**, 052016 (2013).
[5] I. Adachi *et al.* (Belle Collaboration), arXiv:1105.4583.
[6] S. Kurokawa and E. Kikutani, Nucl. Instrum. Methods Phys. Res. Sect., A **499**, 1 (2003), and other papers included in this Volume;T.Abe *et al.* Prog. Theor. Exp. Phys. (2013) 03A001 and following articles up to 03A011.
[7] A. Abashian *et al.* (Belle Collaboration), Nucl. Instrum. Methods Phys. Res., Sect. A **479**, 117 (2002); also see detector section in J. Brodzicka *et al.* Prog. Theor. Exp. Phys. (2012) 04D001.
[8] D. J. Lange, Nucl. Instrum. Methods Phys. Res. A **462**, 152 (2001).
[9] E. Barberio and Z. Wąs, Comput. Phys. Commun. **79**, 291 (1994).
[10] R. Brun *et al.*, GEANT 3.21, CERN DD/EE/84-1, 1984.
[11] J. E. Gaiser, Ph.D. thesis, SLAC-R-255 (1982) (unpublished); T. Skwarnicki, Ph.D. thesis, DESY F31-86-02 (1986) (unpublished).
[12] A. Garmash *et al.* (Belle Collaboration), Phys. Rev. D **71**, 092003 (2005).
[13] M. G. Kendall and A. Stuart, *The Advanced Theory of Statistics*, 2nd ed. (Hafner Publishing, New York, 1968).
[14] J. Beringer *et al.* (Particle Data Group), Phys. Rev. D **86**, 010001 (2012).
[15] E. A. Kuraev, V. S. Fadin, Sov. J. Nucl. Phys. 41, 466 (1985); M. Benayoun, S. I. Eidelman, V. N. Ivanchenko, Z. K. Silagadze, Mod. Phys. Lett. A**14**, 2605 (1999).
[16] K.-F. Chen *et al.* (Belle Collaboration), Phys. Rev. D **82**, 091106 (2010).

[17] S. Actis *et al.*, Eur. Phys. J. C **66**, 585 (2010).
[18] S. Esen *et al.* (Belle Collaboration), Phys. Rev. D **87**, 031101(R) (2013).
[19] A. E. Bondar, A. Garmash, A. I. Milstein, R. Mizuk, M. B. Voloshin, Phys. Rev. D **84**, 054010 (2011);
[20] D.-Y. Chen and X. Liu, Phys. Rev. D **84**, 094003 (2011); A. Ali, C. Hambrock and W. Wang, Phys. Rev. D **85**, 054011 (2012); I. V. Danilkin, V. D. Orlovsky and Y. A. Simonov, Phys. Rev. D **85**, 034012 (2012); S. Ohkoda, Y. Yamaguchi, S. Yasui, K. Sudoh and A. Hosaka, Phys. Rev. D **86**, 014004 (2012); E. Braaten, C. Langmack, D. Hudson Smith arXiv:1402.0438[hep-ph].
[21] A. Garmash *et al.* (Belle Collaboration), Phys. Rev. Lett. **96**, 251803 (2006).
[22] M. B. Voloshin, Prog. Part. Nucl. Phys. **61**, 455 (2008).
[23] M. B. Voloshin, Phys. Rev. D **74**, 054022 (2006).